Am J Nucl Med Mol Imaging 2020;10(5):212-225
www.ajnmmi.us /ISSN:2160-8407/ajnmmi0114368

Original Article

Liver background uptake of [^{18}F]FLT in PET imaging

Olga Sergeeva[1*], Yifan Zhang[1*], Jonathan Kenyon[2], Galen Miller-Atkins[3], Maxim Sergeev[4], Emily Verbus[5], Renuka Iyer[6], Sandra Sexton[6], Vladimir Kepe[7], Norbert Avril[1,4], Yogen Saunthararajah[8], Ernst Ricky Chan[3], Zhenghong Lee[1,4]

Departments of [1]Radiology, [2]Biology, Case Western Reserve University, Cleveland, OH, USA; [3]Institute for Computational Biology, Cleveland, OH, USA; [4]Nuclear Medicine, University Hospitals Cleveland Medical Center, Cleveland, OH, USA; [5]Surgery, University Hospitals Cleveland Medical Center, Cleveland, OH, USA; [6]Medical Oncology, Rowell Park Cancer Center, Buffalo, NY, USA; [7]Nuclear Medicine, Cleveland Clinic, Cleveland, OH, USA; [8]Hematology and Oncology, Cleveland Clinic, Cleveland, OH, USA. [*]Equal contributors.

Received May 14, 2020; Accepted August 29, 2020; Epub October 15, 2020; Published October 30, 2020

Abstract: High liver uptake presents a problem for 3'-deoxy-3'-[^{18}F]fluorothymidine ([^{18}F]FLT) as a radiotracer for imaging cellular proliferation in the liver with positron emission tomography (PET). This investigation re-visited some issues related to the high liver background uptake of [^{18}F]FLT with an animal model of woodchucks. Several enzymes involved in the hepatic catabolism of FLT, thymidine phosphorylase (TP, TYMP), uridine 5'-diphospho-glucuronosyltransferases (UDP-GTs, short for UGTs), and β-glucuronidase (GUSB), their homology as well as hepatic expression between the human and the woodchuck was examined. Inhibitors of these enzymes, TP inhibitor (TPI) tipiracil hydrochloride, UGT inhibitor probenecid, β-glucuronidase inhibitor L-aspartate, were administered to the animals at human equivalent doses either intravenously (i.v.) and orally before the injection of tracer-dose [^{18}F]FLT for PET imaging to examine any changes in liver uptake. Liver tissue samples were harvested from the animals after PET imaging and used to perform polymerase chain reaction (PCR) for TP expression or assays for enzymatic activities of TP and β-glucuronidase. Non-radiolabeled (cold) FLT was also applied for enzyme saturation. Animals administered with TPI displayed lower radioactivity in the liver in comparison with the baseline scan. The application of probenecid did not change [^{18}F]FLT liver uptake even though it reduced renal uptake. L-aspartate reduced the liver background uptake of [^{18}F]FLT slightly. The application of cold FLT reduced overall uptake of [^{18}F]FLT including the liver background. Therefore, the combined application of cold FLT and [^{18}F]FLT merits further clinical investigation for reducing liver background uptake of [^{18}F]FLT.

Keywords: FLT, PET imaging, metabolic enzymes

Introduction

DNA synthesis and renewal of genetic material are essential for cell proliferation. Cells form thymidine monophosphate, a necessary precursor of DNA, either by methylating deoxyuridine monophosphate via the *de novo* pathway or by phosphorylating thymidine imported from the extracellular milieu through the salvage pathway (**Figure 1**). Radiolabeled nucleoside analogs (**Figure 2A**) have been developed for positron emission tomography (PET) imaging of tumor proliferation through the salvage pathway, one of them is 3'-deoxy-3'-[^{18}F]fluorothymidine ([^{18}F]FLT) whose cellular uptake depends on the enzymatic activity of cytosolic thymidine kinase (TK1, **Figure 1**) [1]. TK1-dependent [^{18}F]FLT uptake has been correlated with tumor proliferation in solid neoplasms such as non-small cell lung cancer [2], colorectal cancer [3], breast cancer [4], lymphoma [5], and sarcoma [6]. However, [^{18}F]FLT is not suitable for PET imaging in the liver because of a high liver background uptake seen in the clinical scans as shown in **Figure 2B**. In this study, we re-visited issues associated with the high liver background uptake of [^{18}F]FLT using a unique animal model: viral-hepatitis infection-induced hepatocellular carcinoma (HCC) in the woodchucks [7].

The development of FLT by placing a fluorine on the ribose in place of a hydrogen greatly strengthened the N-glycosidic bond against the cleavage by thymidine phosphorylase (TP, **Figure 1**) [8], and resulted in a more stable [^{18}F]FLT in circulation than the native [^{11}C]thymidine.

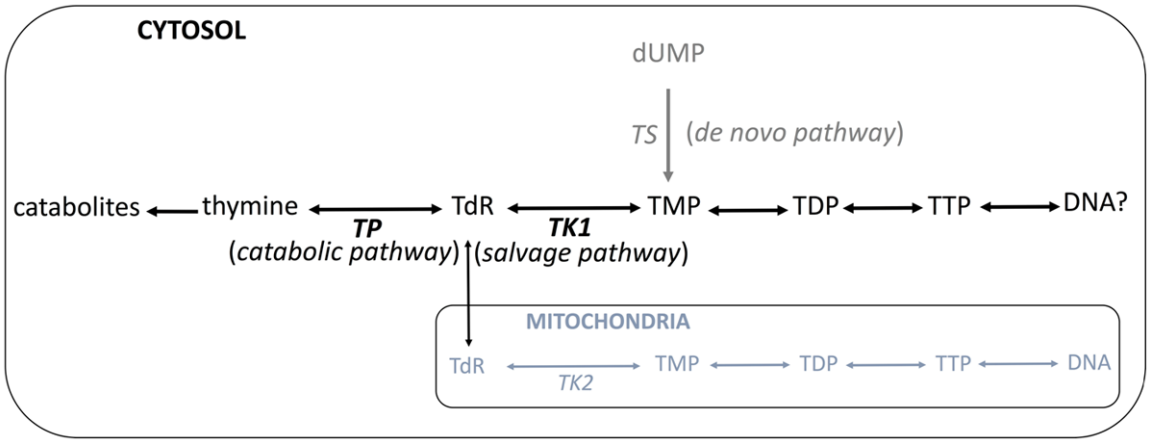

Figure 1. DNA synthesis pathways. Key enzymes are shown in *italic* type. *TS*: thymidine synthase; *TK1*: cytosolic thymidine kinase; *TP*: thymidine phosphorylase; *TK2*: mitochondrial thymidine kinase. TdR: thymidine; dUMP: deoxyuridine monophosphates; TMP: thymidine monophosphate; TDP: thymidine diphosphate; TTP: thymidine triphosphate.

However, the activity of TP in the liver [9] could possibly produce ^{18}F-labeled arabinofranose, which would be metabolized further similarly along the ribose metabolic pathways in the liver and contribute to liver background signal (see Figure S1) [10]. Transient suppression of hepatic TP is required to protect the integrity of certain nucleoside analog drugs such as in the case of TAS-102 (Lonsurf®, Taiho Oncology), which gained FDA approval for refractory metastatic colorectal cancer treatment. TAS-102 is a 2:1 combination of an active ingredient, trifluridine (FTD) and the TP inhibitor (TPI), tipiracil hydrochloride, which maintains FTD integrity against TP in the liver [11]. Working with the woodchuck model, we tested the inhibition of TP in the liver with the same TPI, tipiracil, which transiently suppresses hepatic TP activity despite that [^{18}F]FLT is designed to resist hydrolysis by TP [8], to examine any change in the liver background uptake.

For long, the high hepatic background uptake was attributed to the glucuronidation of [^{18}F]FLT [1] based on the well-documented hepatic glucuronidation of a thymidine analogue 3'-azido-3'-deoxythymidine (AZT, developed for the treatment of HIV-AIDS) [12] by enzymes from the family of uridine 5'-diphospho-glucuronosyltransferases (UDP-GTs or UGTs, **Figure 2C**). Meanwhile little effort has been devoted to the investigation of [^{18}F]FLT glucuronidation or the reduction of the high liver background uptake. We explored possible ways to reduce the background uptake by inhibiting hepatic glucuronidation with probenecid in the woodchuck models. Probenecid is FDA-approved for the treatment of gout. It inhibits renal excretion of some drugs, thereby increasing their plasma concentration to prolong their therapeutic effects [13]. It also inhibits hepatic glucuronidation in a partial non-competitive fashion as exemplified by the inhibition of AZT glucuronidation [14]. In addition, there is β-glucuronidase (GUSB) that reverses the process of glucuronidation (**Figure 2D**), which is mostly active in lysosomes although a fraction resides in the lumen of liver endoplasmic reticulum (ER) while UGT resides in the ER where the glucuronidation takes place (**Figure 2E**). We experimented with a known β-glucuronidase inhibitor L-aspartate to try to break this possible ER loop (**Figure 2D**). L-aspartic acid, a readily available food supplement, was found to be protective of liver by inhibiting gut bacterial GUSB [15]. We tested this nonessential amino acid in an attempt to reduce the hepatic background uptake of [^{18}F]FLT.

Finally, we applied a clinically "safe" dose of non-radiolabeled (cold) FLT shortly before the injection of "hot" [^{18}F]FLT into the woodchuck models to exam any changes in liver background uptake of [^{18}F]FLT. Rodents such as mice showed little liver uptake of [^{18}F]FLT compared to humans due possibly to a higher concentration of endogenous thymidine in circulation [16]. Inspired by this, we tested the saturation of hepatic enzymes responsible for [^{18}F]FLT metabolism/catabolism with cold FLT to reduce the background uptake of [^{18}F]FLT in the liver.

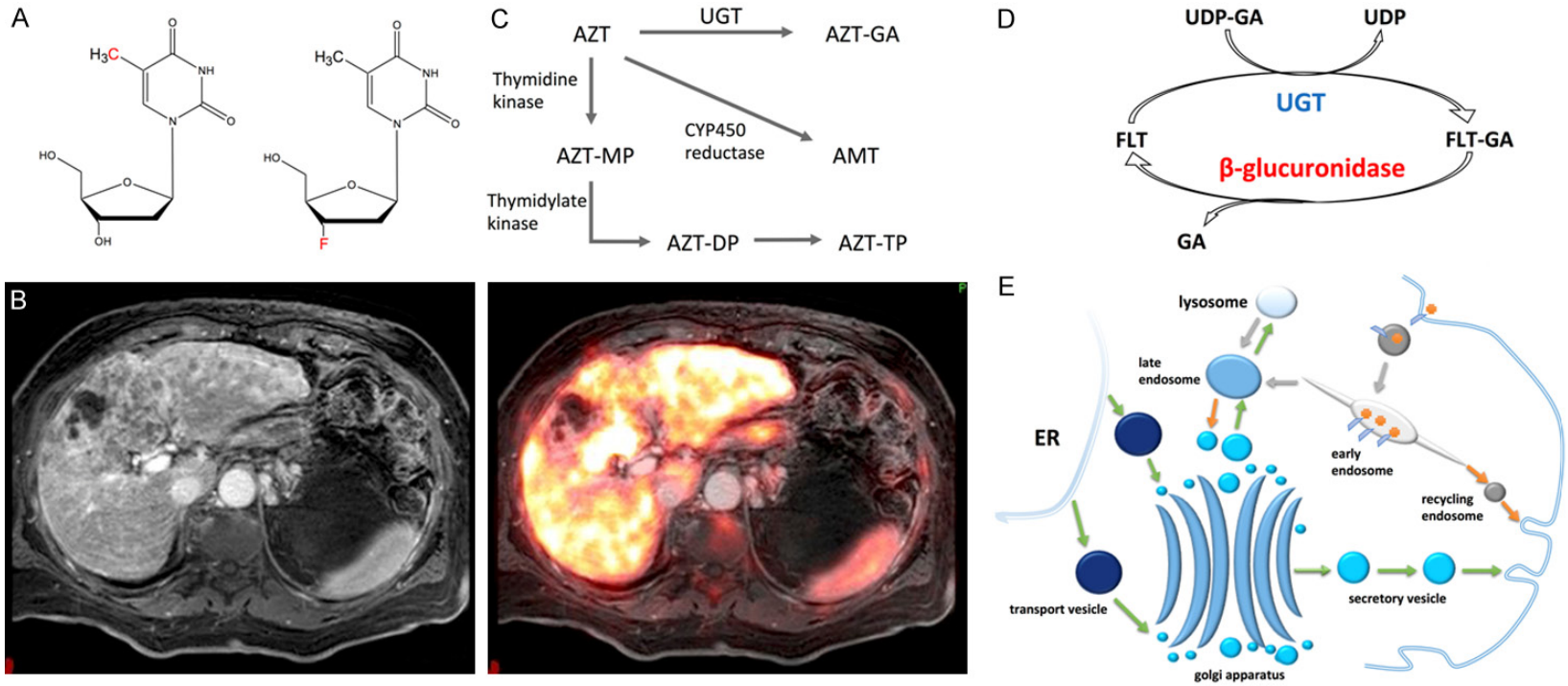

Figure 2. FLT metabolism in the liver. A. C-11 labeled thymidine (TdR) and F-18 labeled FLT; B. Trans-axial MRI of liver cancer (left) and MRI/PET overlay of [18F]FLT (right) taken at 1.0 hr post injection; C. Metabolic pathways for AZT; D. Hypothesized hepatic loop mediated by uridine 5'-diphospho-glucuronosyl-transferases (UGT) and β-glucuronidase (GUSB) in endoplasmic reticulum (ER); E. Sub-cellular localizations of organelles.

Materials and methods

Animal models

Woodchucks weighted 8-10 lbs (averaged 3.5 kg) and aged 2-3 years old were selected at Roswell Park Comprehensive Cancer Center (Buffalo, NY) for shipment to Case Western Reserve University (Cleveland, OH). A venous access port (SAI Infusion Technologies; Elgin, IL) was surgically implanted in each animal to facilitate radiotracer injection in all PET scans. The port was flushed regularly with heparinized saline. The food was taken away 4-5 hours before each PET imaging session for the easy of anesthesia procedure while drinking water was always kept. All procedures are approved by the Institutional Animal Care and Use Committee of the University.

Bioinformatics

Human data from The Cancer Genome Atlas (TCGA) were downloaded from the public TCGA Liver Hepatocellular Carcinoma database (TCGA-LIHC). The data include a total of 371 RNA-seq gene expression results collected from both tumor and non-tumor human tissues. The TCGA-LIHC data were all sequenced using Illumina platforms and available as "raw" (i.e. un-normalized) read counts for each gene for each sample. Data were then reformatted and sent through the DESeq2 workflow in R [17] including a pre-filtering step, where genes with very low gene counts are excluded, a normalization step to aid in comparing genes across samples, calculating the log2 fold change between non-tumor and tumor samples for each gene, and the differential expression between non-tumor and tumor genes with a Wald test. The final results yield the base mean for each gene, the log2 fold change (FC) as tumor over liver, the standard error for the FC, the Wald test statistic, and the raw and adjusted *p*-value for multiple testing correction using the false discovery rate (FDR).

The woodchuck data were collected from the National Center for Biotechnology Information (NCBI) Gene Expression Omnibus (accession number GSE36545 and BioProject PRJNA155585). The data include 102 samples (GSM896624-GSM896725) from 13 woodchucks with a total of 42 tumor samples and 60 non-tumor samples [18]. The data obtained was from a custom NimbleGen Woodchuck Gene Expression HX3 Microarray. The downloaded data are normalized gene expression data for each sample, formatted in parallel to the TCGA dataset although the two sets of data were processed differently due to the difference in the dynamic range inherent to each technology. Nine outlying samples were identified with principal component analysis and subsequently excluded from the analysis. Log2 FC and t-tests were then calculated to compare the gene expression between tumor and non-tumor samples. All resulting *p*-values were FDR corrected to adjust for multiple testing.

The expression of the key genes involved in the metabolism/catabolism of FLT: TYMP (the gene coding TP), UGTs (the genes coding UGT isomers), and GUSB (the gene coding β-glucuronidase) between liver tumors and non-tumor liver tissues were tallied from the databases. The human data came from TCGA, and the woodchuck data from the customized microarray. Homology of amino acid sequences between human ([Homo sapiens]) and woodchuck ([marmot]) proteins was determined by using Protein Basic Local Alignment Search Tool (BLAST) (https://blast.ncbi.nlm.nih.gov/Blast.cgi). For example, the homology between the two species was searched for TYMP (NCBI Reference Sequence: NP_001244917.1 [Homo sapiens] and NCBI Reference Sequence: XP_015362361.1 [Marmota marmota marmota]). Similarly, the homology between the two species was also searched for UGT1A1, UGT1A9, UGT2B4, and UGT2B15, and GUSB, and described in Supplementary Materials.

Radiotracers

For PET imaging, [18F]FLT was synthesized automatically with the Scintomics module (Fürstenfeldbruck, Germany) using the sequence provided by the vendor. For scintigraphy or hepatobiliary iminodiacetic acid (HIDA) scan and single photon emission computerized tomography (SPECT) scan, [99mTc]mebrofenin (trimethylbromo-iminodiaceticacid) was prepared using the Choletec® kit supplied by Bracco (Monroe Township, NJ).

Imaging experiments and data analysis

For the baseline scan, the animal was placed prone in the clinical Ingenuity PET/CT scanner

(Philips, Cleveland, OH) and under 3% isoflurane gas anesthesia throughout the scan. After a low-dose CT scan, 52~80 MBq (1.46~2.1 mCi) [18F]FLT was injected intravenously (i.v.) through the implanted venous access port and followed by a dynamic PET scan of 60 min in list mode on the clinical PET/CT system as the woodchucks with an average weight of 3.5 kg would not fit into the microPET. PET acquisition was re-binned into a total of 21 frames: 10 × 30 seconds, 5 × 1-min, 2 × 5-min frames and 4 × 10 min, respectively. Selected animals also had the HIDA scan until visible signal in the gallbladder (GB). A planar dynamic scintigraphic scan centered on the liver was performed with the Philips Brightview XCT (Cleveland, Ohio) SPECT/CT scanner at the injection of 18.5 MBq (0.5 mCi) [99mTc]mebrofenin, and until GB signal was concentrated. A SPECT/CT scan was then followed immediately on the same clinical scanner for the localization of GB and in comparison with the PET/CT scan for the timing of GB concentrating. Briefly, after the corn-beam low-dose X-Ray CT scan, the SPECT acquisition used a medium energy collimator and 15% energy window around the photopeak, 128 × 128 matrix and 128 projections in total over a full 360° rotation. The vendor-supplied iterative image reconstruction algorithm ordered subset expectation maximization (OSEM) was used to reconstruct the SPECT images.

After the baseline scan, additional PET scans with [18F]FLT were performed identically with the same animal after the application of one of the inhibitors. For TP inhibition, tipiracil at 70 mg/kg was administered i.v. 1-4 min before and orally 4-5 hrs before the injection [18F]FLT injection for PET imaging; for inhibiting hepatic glucuronidation, probenecid at 0.25 g/kg was administered orally 2 hrs before [18F]FLT injection; for β-glucuronidase inhibition, L-aspartic acid at 300 mg/kg once daily was also administered orally for 4 days consecutively before PET imaging with [18F]FLT; for enzymatic saturation, cold FLT applied at 6.0 mg/kg i.v. 10 min before the hot [18F]FLT injection. Four animals were scanned three times in the sequence of baseline, TPI (tipiracil i.v. and oral) applications prior to [18F]FLT injection; three animals were scanned three times in the sequence of baseline, the application of probenecid and cold FLT; two additional animals were compared for [18F]FLT liver uptake, one scanned after 4 days of oral L-aspartate administration at 300 mg/kg once daily, and the other as a control without L-aspartate. All scans for each animal were scheduled within two weeks, but at least 48 hrs apart, giving the time for radio-decay from the last scan, and for animal recovery from anesthesia between the scans. After the final scan, the animals were euthanized for tissue harvesting. The samples were fresh-frozen immediately for later use in quantitative real-time polymerase chain reaction (qRT-PCR) or enzymatic assay.

Standardized uptake value (SUV), which is the normalized radiotracer uptake by body weight and injected dose [19], was calculated based on the circular regions of interest (ROIs) placed in the liver as well as focal uptakes in the kidneys or GB, and time activity curves in the unit of SUV were generated for these ROIs.

qRT-PCR for thymidine phosphorylase (TP or TYMP)

The primers for qRT-PCR were designed at The Custom TaqMan® Assay Design Tool based on marmot mRNA sequences for required genes: TYMP (custom TaqMan gene expression assay AP47WWH based on XM_015506875.1 mRNA sequence), and endogenous control gene GAPDH (assay AP2W9P7 based on XM_015500718.1 mRNA sequence). RNA was extracted from tissue using Qiagen miRNeasy Mini Kit (Cat. No. 217004, Qiagen) according to manufacturer's instructions. Total RNA (0.25 μg for each reaction) was used to generate complementary DNA (cDNA) with the High-Capacity RNA-to-cDNA Kit (Cat. No. 4387406; Applied Biosystems). qRT-PCR was performed on a StepOne Plus real-time thermocycler with 1.33 mL of cDNA for each reaction and the TaqMan Universal master Mix II, with UNG (Cat. No. 4440038; Applied Biosystems). Expression data was obtained for each gene from each sample as threshold cycle (Ct). ΔCt was calculated as the Ct of endogenous control gene minus the Ct of the gene of interest. ΔΔCt was then calculated as the ΔCt of the reference sample minus the ΔCt of another sample. This sets the ΔΔCt of the reference sample to 0. The relative quantification (RQ) of gene expression was calculated as 2-fΔΔCt). This yields an RQ for the reference sample as 1. Samples with more transcripts than the reference sample will have negative ΔΔCt scores and larger RQ values.

Enzymatic assay for thymidine phosphorylase (TP, EC 2.4.2.4)

The TP assay conditions were essentially as described by Marti and colleagues, with a few modifications [20]. Previously frozen animal tissue samples were homogenized using pestle mortar method, and were then added into the lysis buffer containing 50 mM Tris-HCl pH 7.2, 0.1% triton x-100, 0.02% mercaptoethanol, 2 mM PMSF (phenylmethylsulphonylfluoride), and protease inhibitor cocktail. The homogenized samples were passed 2-3 times through 25 G needle, after that the samples were incubated for 30 min on ice and were then centrifuged for 30 min at 28,000 × *g* at 4°C to remove any remaining insoluble material. Protein content was determined using Pierce 660 nm protein assay (Thermo Scientific™, #22660) according to manufacturer's instructions. Supernatants from homogenates, containing 150 µg protein, were incubated with 0.1 M Tris-arsenate buffer (pH 6.5) containing 10 mM thymidine in a total volume of 0.1 mL. After incubation for 1 hour at 37°C, the reaction was stopped by adding 1 mL of 1 ml of 0.55 M perchloric acid and the reaction tube were placed on ice for 5 minutes, causing precipitation of the protein. Then, the samples were either directly prepared for HPLC analysis or stored at -20°C. Reaction blanks were created by performing the acid-precipitation immediately after mixing the cell extract with the reaction solution. Prior to HPLC analysis, the samples were centrifuged for 10 min at 20,000 × *g* at 4°C.

Reaction products were quantified by reversed phase high performance liquid chromatography at ambient temperature using a 100 mm × 4.6 mm Luna 5 um C18(2) column (Phenomenex) at a flow rate of 0.5 ml/min, using water/acetonitrile (95/5) mobile phase. Detection of thymine was performed at 267 nm. Thymidine and thymine concentrations were calculated using pure compounds as standards.

Enzymatic assay for β-glucuronidase (EC 3.2.1.31)

The same frozen liver tissue samples harvested from the woodchucks as in the TP assay were used in this experiment. The following procedures were carried out at 2~4°C unless otherwise indicated. β-Glucuronidase activity was quantified by measuring the hydrolysis rate of the fluorogenic substrate 4-methylumbelliferyl β-D-glucuronide (MUG) (Sigma) as described previously [21]. Briefly, harvested tissues (approximately 50 mg) were homogenized in the lysis buffer (500 ml of 0.2% Triton-saline). Tissue samples were vortexed, then freeze-thawed three times by incubating at -80°C for 30 min. and then thawing at 37°C. The samples were microfuged for 2 min at 12,000 × *g*. 250 mL aliquots were heat-inactivated for 90 min at 65°C. 4-methylumbelliferone (4-MU) standards were made in the range of 0~100 mM for a standard curve. 100 mL of substrate (10 mM 4-methylumbelliferyl β-D-glucuronide (MUGlUc) in 0.1 M NaAc buffer) was combined with 50 mL of sample (or standard) in a 96-well fluorometer plate and incubated at 37°C for 2~4 hrs. The substrate MUGlUc was cleaved in the presence of β-glucuronidase, producing a fluorogenic compound that is easily detected using a fluorometer. All samples and standards were done in triplicate. The reaction was quenched by the addition of a glycine-carbonate buffer (0.32 M glycine, 0.2 M $NaCHO_3$). Samples and standards were read on a CytoFluor fluorometer (Applied Biosystems, Branchburg, NJ) at the wavelengths of 360 nm (excitation) and 450 nm (emission). β-Glucuronidase activity was calculated by first correcting for the blank reading. Standards were averaged and used to calculate the Kf constant ((average of standard/reading) × (1000 mL/mL/100 mL) × (dilution factor)). The samples were assayed after the heat-inactivation step and a subsequent spin of 2 min at 12,000 × *g*. β-Glucuronidase activity was calculated as: nmoles/hr/mg protein = (corrected reading) × Kf × # of hours × (dilution factor, if any). One unit of enzyme activity is expressed as the amount of enzyme that catalyzes the release of 1 nmol of 4-methylumbelliferone/hr. The protein concentration of each sample was determined by a similar protein determination method as in the TP assay. The enzymatic activity is expressed in units per mL of tissue homogenate and then normalized to the total protein content.

Results

UGT1A1, UGT1A9, UGT2B4, and UGT2B15, are the dominant hepatic enzymes from the UGT family: 37% of human UGT1A1 is localized in

Table 1. The expression (base mean counts) of key enzymes in the liver and HCC between the woodchuck and human

	microarray (woodchuck)			RNA-seq (human)		
	liver	HCC	*p*-adjusted	liver	HCC	*p*-adjusted
UGT1A1	13.62426	13.13745	4.23181E-06	8801.71186	3533.46947	1.45163E-05
UGT1A9	13.55701	13.50425	*0.673895776*	2466.35805	1734.90550	*0.142498018*
UGT2B4	13.79634	13.15938	1.90991E-06	45576.22225	41455.97744	*0.589224659*
UGT2B15	11.81149	10.58412	3.53358E-15	19323.67142	12831.68579	0.035838247
TP (TYMP)	8.83511	8.76515	*0.476674647*	3652.80124	5092.15043	0.010859334
GUSB	13.35361	13.61442	0.001676322	8868.19768	7248.33974	0.006082343

the liver; 31% of human UGT1A9 is in the liver; 59% of human UGT2B4 is localized in the liver; 29% of human UGT2B15 is in the liver [22]. These four UGTs showed a homology of 88%, 88%, 52% and 86%, respectively, between human and woodchuck. Noticeably, the predicted marmot UTG2B4 sequence is much shorter than the human UTG2B4 sequence, which resulted in many gaps in the alignment between the two species for UGT2B4, while a higher degree of homology (85%) was found between the woodchuck UGT2B4 and human UGT2B15. The expression of many UGTs is significantly higher in the liver parenchyma than in HCC (**Table 1** showing FC with adjusted *p*-value) from both woodchuck (microarray) and human (RNA-seq) results. Inversely, GUSB (β-glucuronidase) showed dis-concordant expression ratio between liver and HCC among woodchuck and human (**Table 1**) while the differences are rather small, and an 89% homology in protein sequence between the two species was found for GUSB. Likewise, while the results from human samples showed a higher TYMP (TP) expression in HCC than in the surrounding liver parenchyma, and that from woodchuck did not show such a significant difference (**Table 1**). PCR with harvested woodchuck liver tissues using the woodchuck-specific primer for TYMP (TP) showed inconsistent tumor/liver ratios among the four animals (**Figure 3A**). A 92% homology between the two species was found for TYMP. Markedly, the base mean level of GUSB is higher than that of TYMP, which prompted us to check enzymatic activity of the two, as reported next. The FASTA results of TYMP, UGTs and GUSB were included in the Supplementary Materials.

The specific enzyme activity of TP measured from the liver and tumor tissue samples was calculated from the product formed in the reaction and expressed as nanomoles of thymine composed per hour and μg of total protein. After 60 min reaction, the extracts showed similar TP enzymatic activities in the liver tissue and tumor samples (**Figure 3B**). Results using the tissue samples from the other three animals showed no significant difference in enzymatic activities of β-glucuronidase between HCC and its surrounding hepatic tissues with the activities one-order higher than that of TP (**Figure 3C**).

Radiosynthesis using the Scintomics module produced [18F]FLT with a consistent radiochemical yield > 20%, radiochemical purity > 98%. Woodchuck PET imaging using [18F]FLT displayed a sustained high background uptake in the liver after radiotracer clearance cleared from the circulation (**Figure 3D**), which recapitulates the human scans. Clinical grade [99mTc] mebrofenin was prepared for the HIDA scan. Oral gavage of various inhibitors (TPI, probenecid, L-aspartate) before imaging was done when the animal was awake (**Figure 3E**).

Animals administered with TPI reduced liver uptake of [18F]FLT in comparison with that in the baseline scan (**Figure 4**). At 55 min post injection of [18F]FLT, liver SUVs calculated based on the circular ROI were 2.1 after TPI application and 3.5 in the baseline scan, respectively. The gallbladder (GB) concentration showed up earlier, on average 5-6 min after TPI treatment vs. 10 min in the baseline scan (**Figure 4A**). The HIDA scan showed a concentrated GB at about 12 minutes (**Figure 4C**), close to the concentration of GB signal in the baseline PET scans. In addition, there is no difference in timing between i.v. and oral administration of TPI for liver clearance of radioactivity as well as GB concentration (**Figure 4A**, **4D**, **4E**).

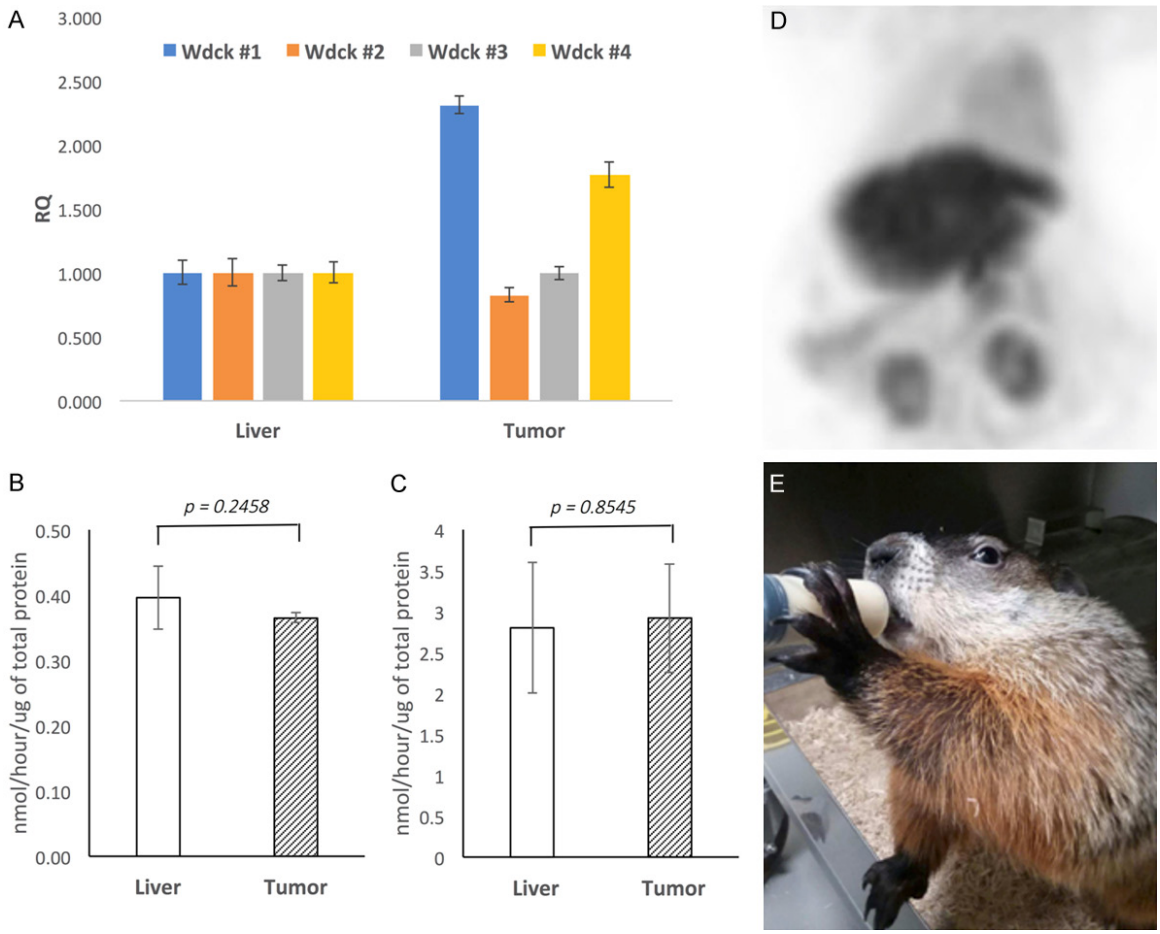

Figure 3. Validating the woodchuck study. (A) PCR results (triplicated) for the expression of expression thymidine phosphorylase (TP) in the samples harvested from 4 woodchucks using the woodchuck primer, the y-axial is relative quantification (RQ) normalized to the liver samples; Comparison of enzymatic activities (in triplicates) between liver tumor and the surrounding hepatic tissues for (B) TP and (C) β-glucuronidase; (D) Coronal maximal intensity projection (MIP) of [18F]FLT PET scan of a woodchuck at 55 min post injection; (E) Oral gavage into a woodchuck.

Comparing to the baseline, the application of probenecid did not alter the level of liver background uptake of [18F]FLT (**Figure 5A**, **5B**) from the baseline scan (**Figure 5C**, **5D**). Noticeably, the renal signal was decreased considerably in comparison and to the anticipated effect of probenecid. Cold FLT application before hot [18F]FLT injection greatly reduced the overall uptake in the liver, kidneys and the gallbladder (**Figure 5E**, **5F**) when comparing to the baseline.

Comparing to the control (Animal 2), after 4 days of large dose of L-aspartate through oral gavage to Animal 1, the liver background uptake of FLT during the PET scan decreased after the initial high peak to an SUV of 3.0 by 55 min post [18F]FLT injection while the SUV of the liver in Animal 2 remained above 4.0 after a lower initial peak. **Figure 6** displays the time activity curves for both animals along with PET/CT overlay of liver uptake at early (initial peak) and later (55 min post-injection).

Discussion

To address the high liver background uptake of [18F]FLT, an early attempt adopted a temporal-intensity information-based voxel-clustering approach, in which the liver background uptake was averaged, and removed through a kinetic spatial filter [23]. This "pure" engineering solution did not take into consideration any biological factors. The clinical studies showed a more complex situation, in which some primary liver tumors with [18F]FLT uptake above the averaged liver background and others below that [24, 25]. To investigate this high liver back-

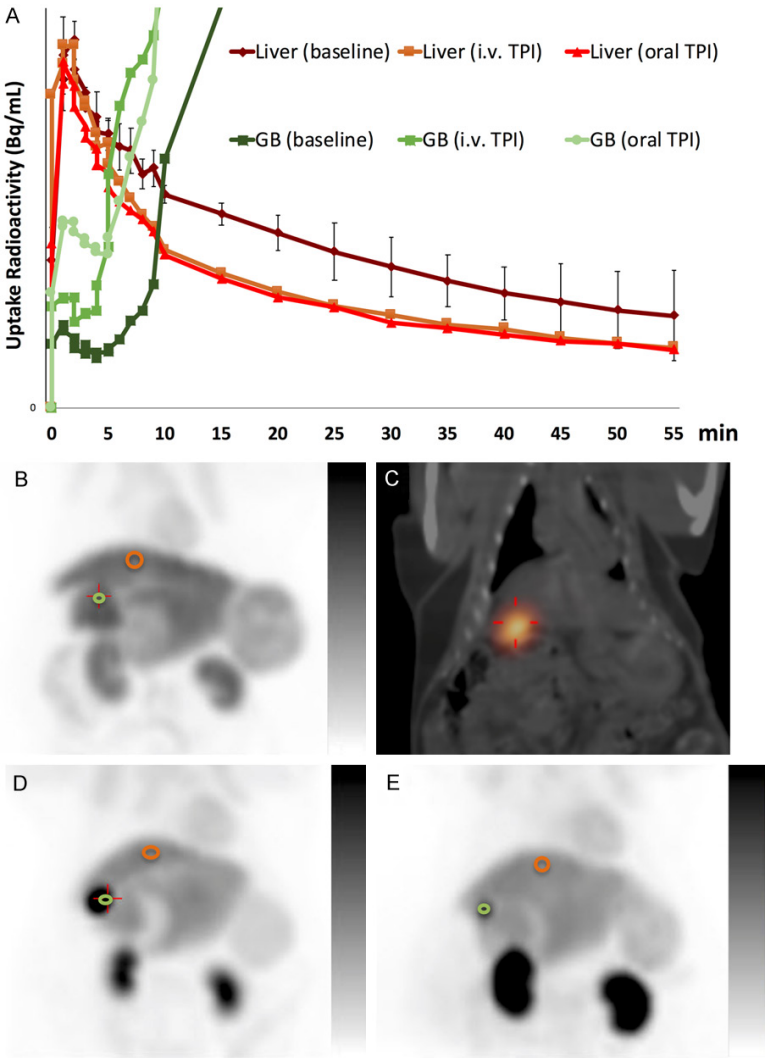

Figure 4. Application of thymidine phosphorylase inhibitor (TPI). (A) Time activity curves of [18F]FLT uptake calculated from the regions of interest (ROIs) placed in liver and gallbladder (GB) at baseline (n=4), after intravenous (i.v., n=3) or oral administration of TPI (n=3), error bars removed for clarity except the baseline liver uptake; (B) A representative MIP of baseline scan [18F]FLT scan with ROIs (orange for liver and green for GB) superimposed; (C) SPECT/CT overlay of HIDA scan taken from the same animal showing GB concentration; The corresponding MIPs of [18F]FLT PET scans after (D) i.v. and (E) oral administration of TPI, also with the ROIs.

ground uptake, an animal model of viral-hepatitis infection-induced HCC in the woodchucks was used. We have examined a list of small molecule radiotracers [26-35] for PET imaging using the same animal model in the past.

As summarized in **Figures 1**, **2**, there are several possible metabolic/catabolic routes that FLT could undergo to produce radiolabeled fragments retained in the liver to present a high background uptake. TP, also known as platelet-derived endothelial cell growth factor (PD-ECGF) [36], was reported to be abundant in the liver for angiogenesis as well as the recycle of thymidine and its analogs [9]. Even though FLT was designed to resist TP cleavage, we applied a known TP inhibitor (TPI), tipiracil (originally developed as an anti-angiogenesis [against PD-ECGF] drug [37], now portion of an FDA approved drug Lonsurf®), with a human equivalent dose before [18F]FLT injection and PET imaging. Previously, a preclinical investigation tested the application of the whole Lonsurf® (2 FTD: 1 TPI), and found a delayed (24 hrs) increase of FLT uptake in xenograft human colorectal carcinoma implicating FTD for stimulating TK activity [38]. However, liver background uptake was not addressed in that study. Our experiment with TPI application resulted in a decreased uptake in the liver comparing to the baseline scan (**Figure 4**). Whether this degree of reduction is enough for clinical PET imaging remains to be tested in future clinical trials. Furthermore, tracer metabolite analysis for [18F]FLT as well as reduction of metabolites by the inhibition of TP will also be part of the investigation and validation in the future. Since oral gavage and i.v. injection of TPI behaved similarly, future clinical trials will have more options for TPI administration before PET imaging.

Glucuronidation of FLT is widely believed to be the main cause for the high liver background uptake following the metabolic study of AZT (**Figure 2C**) [39]. It was estimated that 20% of FLT was glucuronidated in the liver [40]. FLT-glucuronides (FLT-GAs) formed by UGTs was detected in circulation after FLT injection, and glucuronic acid (GA) in FLT-glucuronides was cleaved off with the added β-glucuronidase

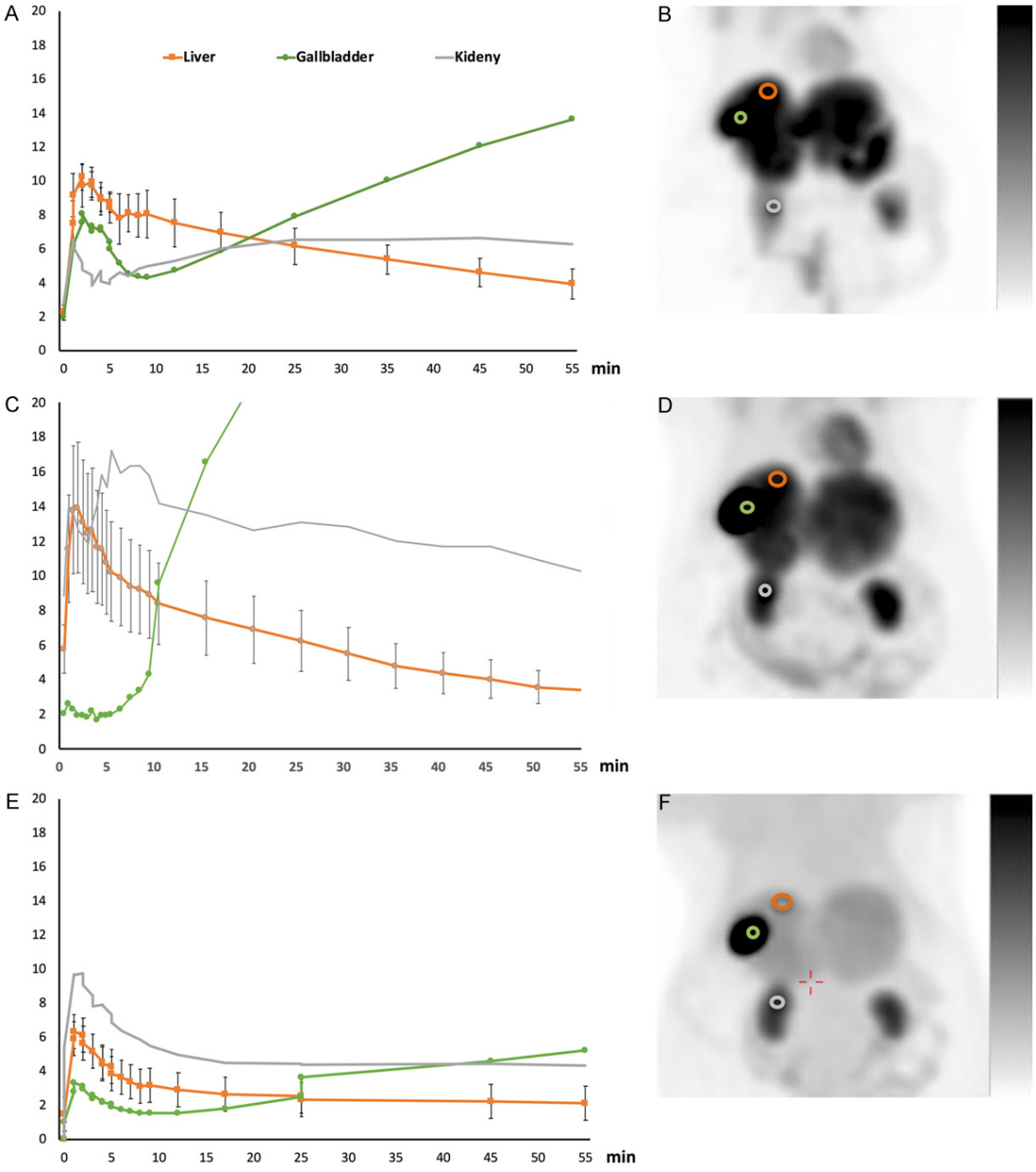

Figure 5. Application of probenecid or FLT. From the top to bottom, [18F]FLT PET scans after oral application of probenecid, at baseline, and after i.v. injection of cold FLT. Left column: representative time activity curves calculated for the ROIs placed in the organs, liver (orange), GB (green) and kidney (grey). Error bars are only shown for the liver uptake for the clarity of the display; Right colum: coronal MIPS with the ROIs for each scan from a presentative animal out of three (n=3).

enzyme in the blood sample [4]. What happened in the liver tissue has not been assayed. After treatment with a human equivalent dose of probenecid, PET imaging with FLT showed renal clearance comparing to the baseline scan demonstrating that probenecid is working according to its original indication (**Figure 5A**, **5B**). However, the liver background signal did not change comparing to the baseline. Concentrating gallbladder signal shown during the PET scan (**Figures 4**, **5**) matches that in the HIDA scan indicating the course of FLT-glucuronides in the PET scans to be similar to that of bilirubin-glucuronides displayed in the

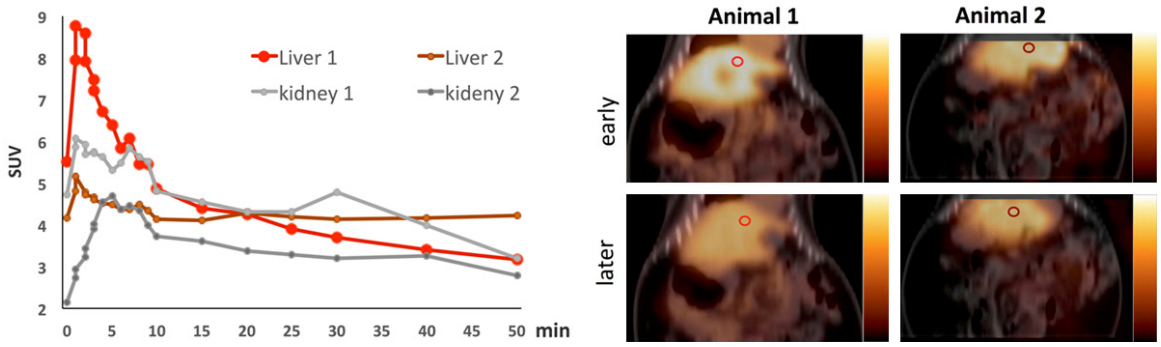

Figure 6. Application of L-aspartate. Animal 1 (Liver 1 and Kidney 1) was fed with L-aspartate for 4 days before PET scan while Animal 2 (Liver 2 and Kidney 2) was the control without L-aspartate. Left: time activity curves calculated with ROIs placed in liver and kidney; Right: coronal PET/CT overlay, with the liver ROI, at early (2 min) and late (55 min) time points.

HIDA scan. Probenecid broadly inhibited many isoforms of UGT in a non-specific manner by inhibiting the clearance of glucuronides [41], which also accumulated as retention to offer a possible explanation for a similar liver background uptake after probenecid application. Perhaps, the new strategy to pursue is to expedite the clearance of hepatic glucuronides with a different intervention to reduce the background signal rapidly.

Another conceivable explanation for the background accumulation is a possible futile cycle between the actions of hepatic UGTs and β-glucuronidase (**Figure 2D**), which would maintain a level of local radioactivity for a high liver background. Inhibition of β-glucuronidase with the application of a food supplement L-aspartate seemed to only lower the liver background slightly (**Figure 6**). L-aspartic acid was found in human milk and cow milk, and was put into commercial infant formula as an ingredient that was found to reduce neonatal jaundice level by inhibiting gut bacterial β-glucuronidase [42]. Whether L-aspartate has any inhibitory effects on hepatic β-glucuronidase cannot be determined from our experiment. Further investigations with more animals are required to draw any conclusions. The precursor of β-glucuronidase is synthesized by membrane-bound ribosome on rough ER, and is subsequently translocated to the ER where post-translational modifications occur [43]. The enzyme undergoes a series of post-translational modifications and the majority is transported to lysosome via the golgi apparatus, see **Figure 2E**. Dual localization of functional β-glucuronidase to ER and lysosome was then discovered [44]. However, given the difference in pH between the acidic lysosome and the near neutral ER, microsomal β-glucuronidase would only have about 10% of lysosomal enzymatic activity [45], hinting a smaller contribution to the possible hepatic hydrolysis of endogenous and xenobiotic glucuronides in ER. This undercuts our hypothesized futile cycle between UGTs and β-glucuronidase due to their mismatched enzyme activities in ER. While the enzymatic assays (**Figure 3**) showed an overall higher β-glucuronidase activity than that of TP in the liver, which is in accordance with the level of expressions of GUSB (β-glucuronidase) and TYMP (TP) in the liver (**Table 1**), the high activity/expression might represent a combination from both microsomal (ER, lower activity) and lysosomal (higher activity) β-glucuronidase. Future cellular metabolite/catabolite analysis will provide hard evidence about the relative amount of glucuronides and other labeled products in organelles. Of note, both TYMP (TP) and GUSB (β-glucuronidase) showed discordant results processed based on the publically available human and woodchuck sequencing data. While PCR revealed large variations among the animals, enzyme assays exhibited no difference in enzymatic activities for both TP and β-glucuronidase between the tumor and the surrounding liver tissues. Therefore, similar inhibitory effects were expected to be applied to both the liver and tumor tissues by TPI and L-aspartate, respectively.

The rodents have no problem with liver background uptake of [18F]FLT as a higher concentration of circulating thymidine in murine, 2-3 orders higher than humans, helped to saturate

the metabolic enzymes and lower the background uptake of FLT in the mouse liver during microPET imaging [16]. Based on this, the cold FLT was applied before the hot [18F]FLT injection and PET imaging in this study. The development of cold FLT, a potent nucleotide reverse transcriptase inhibitor designed for the treatment of multi-resistant HIV, was discontinued due to hepatic toxicity [46]. A dose of FLT at 7.5 mg/kg/day for four weeks produced no toxicity in humans while still reducing the viral load by 1 log [46]. Our study used a single dose of FLT below that of tolerable human equivalent dose before the tracer dose [18F]FLT injection and PET imaging, which decreased [18F]FLT uptake in all organs in the woodchucks. Our specific objective is to enable [18F]FLT for PET imaging of liver cancer proliferation to benefit the management of patients with HCC while avoiding the toxicity associated with FLT. Pre-administration of cold FLT for PET imaging with [18F]FLT is different from cycles of anti-viral treatment with FLT, perhaps a higher single dose of FLT can be considered. However, future clinical studies need to be carefully designed to validate the findings of this preclinical investigation due to the known safety issue with FLT. Besides the safe issue, whether the higher dose of FLT before [18F]FLT injection for PET imaging would also suppress the target TK1 in tumor needs to be tested clinically even though murine studies demonstrated outstanding TK1 activity for microPET imaging despite of a much higher concentration of endogenous thymidine in circulation. Strangely, this cannot be tested with the woodchuck model due to a species-specific defect in TK1 expression albeit TK1 exists in the woodchuck genome [47]. Fortuitously, the rest of hepatic enzymes involved with FLT metabolism in the liver are intact in the woodchucks and mirror those in the humans as demonstrated. It should be noted that a relatively small groups of animals were used in intervention experiments, and only a single animal was treated with L-aspartate along with a control. Hence, the results should be interpretated with caution. Ultimately, we hope to use [18F]FLT-PET to indicate which liver cancer patients may benefit from a therapy with identification of an early response to that treatment.

Acknowledgements

The authors thank the staff from Case Western Reserve University's Animal Resources Center for animal handling, and the staff from Nuclear Medicine of University Hospitals Cleveland Medical Center for SPECT/CT and PET/CT scans. We thank Dr. Agata Exner for providing Illustration for **Figure 2E**. This study was supported in part by NIH R01 CA204373.

Disclosure of conflict of interest

None.

Address correspondence to: Zhenghong Lee, Department of Radiology, Case Western Reserve University, 11100 Euclid Ave, Cleveland, OH 44106, USA. Tel: +216-844-7920; E-mail: zxl11@case.edu

References

[1] Shields AF, Grierson JR, Dohmen BM, Machulla HJ, Stayanoff JC, Lawhorn-Crews JM, Obradovich JE, Muzik O and Mangner TJ. Imaging proliferation in vivo with [F-18]FLT and positron emission tomography. Nat Med 1998; 4: 1334-1336.

[2] Buck AK, Schirrmeister H, Hetzel M, Von Der Heide M, Halter G, Glatting G, Mattfeldt T, Liewald F, Reske SN and Neumaier B. 3-deoxy-3-[(18)F]fluorothymidine-positron emission tomography for noninvasive assessment of proliferation in pulmonary nodules. Cancer Res 2002; 62: 3331-3334.

[3] Francis DL, Freeman A, Visvikis D, Costa DC, Luthra SK, Novelli M, Taylor I and Ell PJ. In vivo imaging of cellular proliferation in colorectal cancer using positron emission tomography. Gut 2003; 52: 1602-1606.

[4] Kenny LM, Vigushin DM, Al-Nahhas A, Osman S, Luthra SK, Shousha S, Coombes RC and Aboagye EO. Quantification of cellular proliferation in tumor and normal tissues of patients with breast cancer by [18F]fluorothymidine-positron emission tomography imaging: evaluation of analytical methods. Cancer Res 2005; 65: 10104-10112.

[5] Buck AK, Bommer M, Stilgenbauer S, Juweid M, Glatting G, Schirrmeister H, Mattfeldt T, Tepsic D, Bunjes D, Mottaghy FM, Krause BJ, Neumaier B, Dohner H, Moller P and Reske SN. Molecular imaging of proliferation in malignant lymphoma. Cancer Res 2006; 66: 11055-11061.

[6] Buck AK, Herrmann K, Buschenfelde CM, Juweid ME, Bischoff M, Glatting G, Weirich G, Moller P, Wester HJ, Scheidhauer K, Dechow T, Peschel C, Schwaiger M and Reske SN. Imaging bone and soft tissue tumors with the proliferation marker [18F]fluorodeoxythymidine. Clin Cancer Res 2008; 14: 2970-2977.

[7] Tennant BC, Toshkov IA, Peek SF, Jacob JR, Menne S, Hornbuckle WE, Schinazi RD, Korba

BE, Cote PJ and Gerin JL. Hepatocellular carcinoma in the woodchuck model of hepatitis B virus infection. Gastroenterology 2004; 127: S283-293.
[8] Fukushima M, Suzuki N, Emura T, Yano S, Kazuno H, Tada Y, Yamada Y and Asao T. Structure and activity of specific inhibitors of thymidine phosphorylase to potentiate the function of antitumor 2'-deoxyribonucleosides. Biochem Pharmacol 2000; 59: 1227-1236.
[9] Boschetti E, D'Alessandro R, Bianco F, Carelli V, Cenacchi G, Pinna AD, Del Gaudio M, Rinaldi R, Stanghellini V, Pironi L, Rhoden K, Tugnoli V, Casali C and De Giorgio R. Liver as a source for thymidine phosphorylase replacement in mitochondrial neurogastrointestinal encephalomyopathy. PLoS One 2014; 9: e96692.
[10] Bijnsdorp IV, Peters GJ, Temmink OH, Fukushima M and Kruyt FA. Differential activation of cell death and autophagy results in an increased cytotoxic potential for trifluorothymidine compared to 5-fluorouracil in colon cancer cells. Int J Cancer 2010; 126: 2457-2468.
[11] Mayer RJ, Van Cutsem E, Falcone A, Yoshino T, Garcia-Carbonero R, Mizunuma N, Yamazaki K, Shimada Y, Tabernero J, Komatsu Y, Sobrero A, Boucher E, Peeters M, Tran B, Lenz HJ, Zaniboni A, Hochster H, Cleary JM, Prenen H, Benedetti F, Mizuguchi H, Makris L, Ito M and Ohtsu A; RECOURSE Study Group. Randomized trial of TAS-102 for refractory metastatic colorectal cancer. N Engl J Med 2015; 372: 1909-1919.
[12] Fischl MA, Richman DD, Grieco MH, Gottlieb MS, Volberding PA, Laskin OL, Leedom JM, Groopman JE, Mildvan D, Schooley RT, et al. The efficacy of azidothymidine (AZT) in the treatment of patients with AIDS and AIDS-related complex. A double-blind, placebo-controlled trial. N Engl J Med 1987; 317: 185-191.
[13] Stewart CF, Fleming RA, Germain BF, Seleznick MJ and Evans WE. Aspirin alters methotrexate disposition in rheumatoid arthritis patients. Arthritis Rheum 1991; 34: 1514-1520.
[14] Qian MX, Finco TS, Mehta M, Viswanathan CT and Gallo JM. Pharmacokinetic evaluation of drug interactions with zidovudine. I: probenecid and zidovudine in monkeys. J Pharm Sci 1991; 80: 1007-1011.
[15] Lin XB, Farhangfar A, Valcheva R, Sawyer MB, Dieleman L, Schieber A, Ganzle MG and Baracos V. The role of intestinal microbiota in development of irinotecan toxicity and in toxicity reduction through dietary fibres in rats. PLoS One 2014; 9: e83644.
[16] Kim W, Le TM, Wei L, Poddar S, Bazzy J, Wang X, Uong NT, Abt ER, Capri JR, Austin WR, Van Valkenburgh JS, Steele D, Gipson RM, Slavik R, Cabebe AE, Taechariyakul T, Yaghoubi SS, Lee JT, Sadeghi S, Lavie A, Faull KF, Witte ON, Donahue TR, Phelps ME, Herschman HR, Herrmann K, Czernin J and Radu CG. [18F]CFA as a clinically translatable probe for PET imaging of deoxycytidine kinase activity. Proc Natl Acad Sci U S A 2016; 113: 4027-4032.
[17] Love MI, Huber W and Anders S. Moderated estimation of fold change and dispersion for RNA-seq data with DESeq2. Genome Biol 2014; 15: 550.
[18] Fletcher SP, Chin DJ, Ji Y, Iniguez AL, Taillon B, Swinney DC, Ravindran P, Cheng DT, Bitter H, Lopatin U, Ma H, Klumpp K and Menne S. Transcriptomic analysis of the woodchuck model of chronic hepatitis B. Hepatology 2012; 56: 820-830.
[19] Julyan PJ, Taylor JH, Hastings DL, Williams HA and Zweit J. SUVpeak: a new parameter for quantification of uptake in FDG PET. Nucl Med Commun 2004; 25: 407.
[20] Marti R, Lopez LC and Hirano M. Assessment of thymidine phosphorylase function: measurement of plasma thymidine (and deoxyuridine) and thymidine phosphorylase activity. Methods Mol Biol 2012; 837: 121-133.
[21] Islam MR, Grubb JH and Sly WS. C-terminal processing of human beta-glucuronidase. The propeptide is required for full expression of catalytic activity, intracellular retention, and proper phosphorylation. J Biol Chem 1993; 268: 22627-22633.
[22] Wu B, Kulkarni K, Basu S, Zhang S and Hu M. First-pass metabolism via UDP-glucuronosyltransferase: a barrier to oral bioavailability of phenolics. J Pharm Sci 2011; 100: 3655-3681.
[23] Contractor K, Challapalli A, Tomasi G, Rosso L, Wasan H, Stebbing J, Kenny L, Mangar S, Riddle P, Palmieri C, Al-Nahhas A, Sharma R, Turkheimer F, Coombes RC and Aboagye E. Imaging of cellular proliferation in liver metastasis by [18F]fluorothymidine positron emission tomography: effect of therapy. Phys Med Biol 2012; 57: 3419-3433.
[24] Eckel F, Herrmann K, Schmidt S, Hillerer C, Wieder HA, Krause BJ, Schuster T, Langer R, Wester HJ, Schmid RM, Schwaiger M and Buck AK. Imaging of proliferation in hepatocellular carcinoma with the in vivo marker 18F-fluorothymidine. J Nucl Med 2009; 50: 1441-1447.
[25] Zhang CC, Yan Z, Li W, Kuszpit K, Painter CL, Zhang Q, Lappin PB, Nichols T, Lira ME, Affolter T, Fahey NR, Cullinane C, Spilker M, Zasadny K, O'Brien P, Buckman D, Wong A and Christensen JG. [(18)F]FLT-PET imaging does not always "light up" proliferating tumor cells. Clin Cancer Res 2012; 18: 1303-1312.
[26] Kolthammer JA, Corn DJ, Tenley N, Wu C, Tian H, Wang Y and Lee Z. PET imaging of hepatocellular carcinoma with 18F-fluoroethylcholine

and 11C-choline. Eur J Nucl Med Mol Imaging 2011; 38: 1248-1256.
[27] Kuang Y, Salem N, Corn DJ, Erokwu B, Tian H, Wang F and Lee Z. Transport and metabolism of radiolabeled choline in hepatocellular carcinoma. Mol Pharm 2010; 7: 2077-2092.
[28] Kuang Y, Salem N, Tian H, Kolthammer JA, Corn DJ, Wu C, Wang F, Wang Y and Lee Z. Imaging lipid synthesis in hepatocellular carcinoma with [methyl-11c]choline: correlation with in vivo metabolic studies. J Nucl Med 2011; 52: 98-106.
[29] Salem N, Kuang Y, Corn D, Erokwu B, Kolthammer JA, Tian H, Wu C, Wang F, Wang Y and Lee Z. [(Methyl)1-(11)c]-acetate metabolism in hepatocellular carcinoma. Mol Imaging Biol 2011; 13: 140-151.
[30] Kuang Y, Wang F, Corn DJ, Tian H and Lee Z. In vitro characterization of uptake mechanism of L-[methyl-H]-methionine in Hepatocellular Carcinoma. Mol Imaging Biol 2014; 16: 459-68.
[31] Kuang Y, Wang F, Corn DJ, Tian H and Lee Z. Metabolism of radiolabeled methionine in hepatocellular carcinoma. Mol Imaging Biol 2014; 16: 44-52.
[32] Kuang Y, Salem N, Wang F, Schomisch SJ, Chandramouli V and Lee Z. A colorimetric assay method to measure acetyl-CoA synthetase activity: application to woodchuck model of hepatitis virus-induced hepatocellular carcinoma. J Biochem Biophys Methods 2007; 70: 649-655.
[33] Kuang Y, Schomisch SJ, Chandramouli V and Lee Z. Hexokinase and glucose-6-phosphatase activity in woodchuck model of hepatitis virus-induced hepatocellular carcinoma. Comp Biochem Physiol C Toxicol Pharmacol 2006; 143: 225-231.
[34] Salem N, Kuang Y, Wang F, Maclennan GT and Lee Z. PET imaging of hepatocellular carcinoma with 2-deoxy-2[18F]fluoro-D-glucose, 6-deoxy-6[18F] fluoro-D-glucose, [1-11C]-acetate and [N-methyl-11C]-choline. Q J Nucl Med Mol Imaging 2009; 53: 144-156.
[35] Tenley N, Corn D, Yuan L and Lee Z. The effect of fasting on acetate PET imaging of hepatocellular carcinoma. J Cancer Ther 2013; 4: 561-567.
[36] Deves C, Rostirolla DC, Martinelli LK, Bizarro CV, Santos DS and Basso LA. The kinetic mechanism of human thymidine phosphorylase - a molecular target for cancer drug development. Mol Biosyst 2014; 10: 592-604.
[37] Takao S, Akiyama SI, Nakajo A, Yoh H, Kitazono M, Natsugoe S, Miyadera K, Fukushima M, Yamada Y and Aikou T. Suppression of metastasis by thymidine phosphorylase inhibitor. Cancer Res 2000; 60: 5345-5348.
[38] Lee HJ, Oh SJ, Lee EJ, Chung JH, Kim Y, Ryu JS, Kim SY, Lee SJ, Moon DH and Kim TW. Positron emission tomography imaging of human colon cancer xenografts in mice with [18F]fluorothymidine after TAS-102 treatment. Cancer Chemother Pharmacol 2015; 75: 1005-1013.
[39] Nicolas F, De Sousa G, Thomas P, Placidi M, Lorenzon G and Rahmani R. Comparative metabolism of 3'-azido-3'-deoxythymidine in cultured hepatocytes from rats, dogs, monkeys, and humans. Drug Metab Dispos 1995; 23: 308-313.
[40] Frings V, van der Veldt AA, Boellaard R, Herder GJ, Giovannetti E, Honeywell R, Peters GJ, Thunnissen E, Hoekstra OS and Smit EF. Pemetrexed induced thymidylate synthase inhibition in non-small cell lung cancer patients: a pilot study with 3'-deoxy-3'-[(1)(8)F]fluorothymidine positron emission tomography. PLoS One 2013; 8: e63705.
[41] Uchaipichat V, Mackenzie PI, Guo XH, Gardner-Stephen D, Galetin A, Houston JB and Miners JO. Human udp-glucuronosyltransferases: isoform selectivity and kinetics of 4-methylumbelliferone and 1-naphthol glucuronidation, effects of organic solvents, and inhibition by diclofenac and probenecid. Drug Metab Dispos 2004; 32: 413-423.
[42] Kreamer BL, Siegel FL and Gourley GR. A novel inhibitor of beta-glucuronidase: L-aspartic acid. Pediatr Res 2001; 50: 460-466.
[43] Naz H, Islam A, Waheed A, Sly WS, Ahmad F and Hassan I. Human beta-glucuronidase: structure, function, and application in enzyme replacement therapy. Rejuvenation Res 2013; 16: 352-363.
[44] Birkenmeier EH, Davisson MT, Beamer WG, Ganschow RE, Vogler CA, Gwynn B, Lyford KA, Maltais LM and Wawrzyniak CJ. Murine mucopolysaccharidosis type VII. Characterization of a mouse with beta-glucuronidase deficiency. J Clin Invest 1989; 83: 1258-1266.
[45] Schollhammer I, Poll DS and Bickel MH. Liver microsomal beta-glucuronidase and UDP-glucuronyltransferase. Enzyme 1975; 20: 269-276.
[46] Georgopapadakou N. Discontinued drugs in 2005: anti-infectives. Expert Opin Investig Drugs 2007; 16: 1-10.
[47] Maschke J, Menne S, Jacob JR, Kreuzfelder E, Tennant BC, Roggendorf M and Grosse-Wilde H. Thymidine utilization abnormality in proliferating lymphocytes and hepatocytes of the woodchuck. Vet Immunol Immunopathol 2001; 78: 279-296.

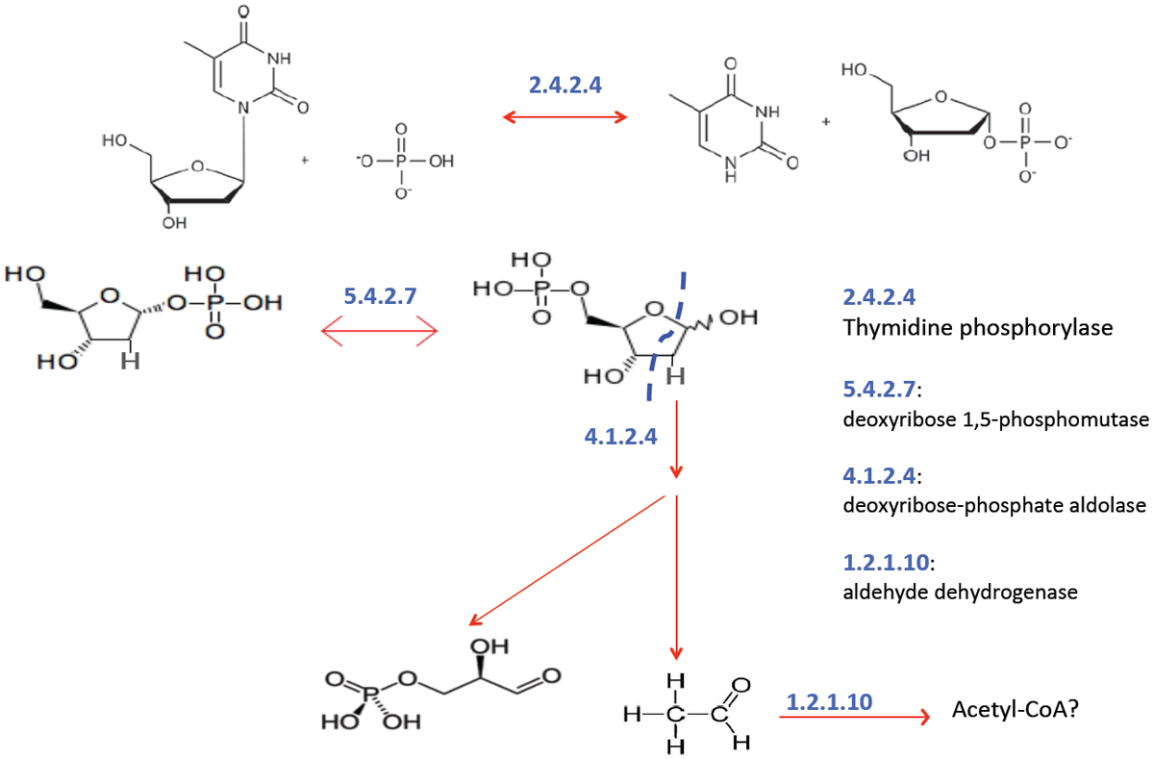

Figure S1. Possible metabolic pathways of ribose in the liver.